Chinese Chemical Letters 33 (2022) 4185–4190

Contents lists available at ScienceDirect

Chinese Chemical Letters

journal homepage: www.elsevier.com/locate/cclet

The effect of organic ligand modification on protein corona formation of nanoscale metal organic frameworks

Wenhao Wang[a,1], Huihui Liu[a,1], Zhengwei Huang[b,*], Fangqin Fu[b], Wenhua Wang[a], Linjing Wu[b], Ying Huang[b,*], Chuanbin Wu[b], Xin Pan[a,*]

[a] School of Pharmaceutical Sciences, Sun Yat-sen University, Guangzhou 510006, China
[b] College of Pharmacy, Jinan University, Guangzhou 511443, China

ARTICLE INFO

Article history:
Received 12 November 2021
Revised 11 February 2022
Accepted 18 February 2022
Available online 22 February 2022

Keywords:
Protein corona
NMOFs
UIO66
Organic ligand modification
BSA

ABSTRACT

Nanoscale metal organic frameworks (NMOFs) have been widely reported in biomedical field for their unique porous structure and tunable multifunctionality. However, when administrated *in vivo*, the protein corona will be formed on the surface of NMOFs, significantly affecting their biodistribution, pharmacokinetics and drug release. Few studies paid attention to the protein corona formation process and its influencing factors of NMOFs. As a well-established strategy for altering structure features of NMOFs, the organic ligand modification may have effect on the protein corona formation process, which is to be investigated. In this study, the zirconium (Zr)-based UIO66 was chosen as model NMOFs, the organic ligand of which was modified with amino group (-NH_2) or carboxyl group (-COOH) to synthesize UIO66-NH_2 and UIO66-2COOH, respectively. Bovine serum albumin (BSA) was chosen as model protein to investigate the protein corona formation process of NMOFs. The current results showed that the -COOH modification remarkably enhanced the BSA adsorption on NMOFs while -NH_2 slightly decreased the protein binding affinity. These differences may be ascribed to the two different dominate protein corona formation modes, *i.e.*, surface coating mode and porous embedded mode. The protein corona formation did not affect the crystal phase of NMOFs but increased the content of α-helix of BSA. Ultimately, upon protein corona formation, the cellular uptake of NMOFs was significantly affected. We believe our study will provide a new research paradigm to the design and applications of NMOFs.

© 2022 Published by Elsevier B.V. on behalf of Chinese Chemical Society and Institute of Materia Medica, Chinese Academy of Medical Sciences.

With the booming development of disease pathology and biomedical materials, great attentions have been paid to nanomedicines due to their multifunctional properties, precise drug delivery and improved therapeutical effect [1]. Varieties of nanoparticles (NPs), including liposomes [2], nanomicelles [3], solid lipid nanoparticles [4], mesoporous silica nanoparticles [5] and nanoscale metal-organic frameworks (NMOFs) [6], were proved to be promising nanoscale drug carriers for multiple disease therapy. However, accumulating evidences have revealed that the NPs will encounter complicated and diversified biological fluids when administrated, which makes their *in vivo* fate remains unknown [7]. Tremendous attention has been paid to the formation of protein corona, a phenomenon where biomolecules in biological fluids like proteins inevitably bind to the surface of NPs and change the biological identity of the pristine NPs [8]. Compared to bare NPs, the protein corona coated NPs may be eliminated by the mononuclear phagocytic system more quickly, affecting the biodistribution and pharmacokinetic profile [9]. Besides, other studies draw different conclusions that the protein adsorption may decrease the NPs-cell membrane adhesion and reduces the cell uptake by altering the surface chemistry of NPs, which may compromise the therapeutical effect of NPs [10,11]. In addition, upon interaction and adsorption on NPs surface, the secondary structures and physiological functions of proteins may also be profoundly affected [12], which may induce nanotoxicity outcomes. Thus, the formation of protein corona and its impacts are considered as one of the keystones to the gap between in vitro design and *in vivo* therapeutic effects of NPs.

Amounting studies have been taken about protein corona formation behaviors of NPs, trying to figure out its fundamental principles and provide guides to nanomedicines design [13]. However, these researches are mainly focused on metal nanoparticles [14] and organic nanoparticles [15]. As a unique emerging organic–

* Corresponding authors.
E-mail addresses: huangzhengw@jnu.edu.cn (Z. Huang), huangy2007@jnu.edu.cn (Y. Huang), panxin2@mail.sysu.edu.cn (X. Pan).
[1] These authors contributed equally to this work.

https://doi.org/10.1016/j.cclet.2022.02.052
1001-8417/© 2022 Published by Elsevier B.V. on behalf of Chinese Chemical Society and Institute of Materia Medica, Chinese Academy of Medical Sciences.

inorganic hybrid biomedical nanomaterial, the studies of NMOFs protein corona are still obscure, including the mechanisms of protein adsorption on NMOFs and the crucial influencing factors. Thus, to accelerate the biomedical applications of NMOFs, a comprehensive understanding of the protein corona formation process is required.

NMOFs were kind of hybrid inorganic-organic materials with periodic structure and porous interior, which was self-assembled by the coordination bond between the metal center and the bridging organic ligand [16]. Recently, the biomedical potentials of NMOFs were found and applied. Equipped with tunable channels, the NMOFs with porous structures allowed them to efficiently load active agents like small molecular drugs, biomacromolecules, photosensitizers and so on [17,18]. In addition, by regulating the metal centers or organic ligand compositions, the NMOFs could be modified to be smart and multifunctional drug delivery systems [19]. Hence, the applications of NMOFs in the biomedical field are in ascendancy and have broad prospects.

The few published studies focus on NMOFs protein corona only elucidate the effect of NMOFs morphology on model protein adsorption [20], the nanotoxicity of plasma incubating NMOFs [21] and colloid stability of NMOFs with protein corona [22]. The impacts of organic ligand, one of the key compositions of NMOFs, on protein corona formation are still a 'black box'. The modification of organic ligands is a commonly employed strategy to alter NMOFs properties, regulating its functions to realize superior drug delivery functions. Modified with active groups like amino group (-NH_2) or carboxyl group (-COOH), the organic ligand can further be conjugated with trigger-responsive bonds or therapeutical agents, improving the application potentials [18]. For example, Gao *et al.* prepared UIO66-NH_2 to conjunct molecular beacons to enhance endogenous RNA imaging [23]. Fan *et al.* prepared the immunoadjuvant functionalized MIL101 NMOFs through -NH_2 modification to improve photo-immunotherapy [24]. Kahn *et al.* employed amino terephthalic acid (with -COOH modification) as organic ligand to build Zn-based MOFs for DNA functionalization [25]. Hence, a systematic study should be performed to fully understand the detailed mechanism and potential impact of protein corona formation of NMOFs with organic ligand modifications.

Thus, in the proposed paper, a single protein model of NMOFs corona study was carried out. Bovine serum albumin (BSA) was chosen as model protein for its abundant *in vivo* content, high stability and excellent intrinsic spectroscopic properties [12]. As the widely studied model NMOFs, UiO66 NMOFs are built up from inorganic zirconium (Zr)-containing octahedra [$Zr_6O_4(OH)_4$] connected by twelve terephthalic acid (BDC) organic ligands to form a microporous structure [26]. Due to its high aqueous stability, easy surface modification and excellent biocompatibility, UIO66 NMOFs were reported as drug carriers for cancer therapy [27–29]. More importantly, the unique BDC ligand of UIO66 allows it appropriate to modification, favoring our proposed research. Through investigating the BSA adsorption on UIO66, UIO66-NH_2 and UIO66-2COOH, the different interaction affinities and protein corona formation modes were revealed and discussed.

The NMOFs were carefully dispersed in HEPES buffer solution, the size distribution and zeta potential of which were accurately measured. As shown in Fig. 1A, the UIO66 NMOFs were nanoscale and have a narrow size distribution. After organic ligand modification with -NH_2 or -COOH, the NMOFs remain nanoscale in diameter and homogeneous distribution, suggesting a negligible impact on NMOFs size. The zeta potential of NMOFs was determined at the same time (Fig. 1B). The negative surface potentials were exhibited in all NMOFs groups. With -NH_2 modification, the zeta potential values of NMOFs were slightly increased, while the opposite behavior was shown with −2COOH modification. Then, FTIR spectra of NMOFs were collected to confirm the chemical structure of NMOFs (Fig. 1C). The characteristic peaks of UIO66-2COOH at 1710 cm^{-1} can be attributed to the C=O stretching vibration of free carboxyl groups, which verifies the success in carboxylation of UIO66. Furthermore, the C–N stretching of UIO66-NH_2 could be reflected by peaks at 1260 cm^{-1}, proving the NH_2 modification of organic ligand [20]. Next, PXRD and TEM were employed to confirm the crystal phase and morphology of NMOFs. UIO66 presented characteristic peaks at 2θ of 7.10°, 8.20°, 11.72°, 13.80°, 25.42°, while Bragg peaks of UIO66-NH_2 (7.10°, 8.18°, 11.70°, 13.80°, 25.40°) and UIO66-2COOH (7.56°, 11.72°, 13.98°, 26.28°) were also clearly shown, indicating the matched crystalline patterns of the corresponding NMOFs (Figs. 1D-F) [30]. The TEM images further indicated the nanoscale of NMOFs (Fig. 1D-F, insertion). These results collaboratively proved the successful synthesis of NMOFs.

The interaction between NMOFs and BSA was firstly confirmed by in situ fluorescence quenching assay, a typical method to evaluate the nanoparticle-protein interaction [12,31]. With excitation at 280 nm, BSA exhibited intrinsic fluorescence due to its two tryptophan (Trp) residues (Trp-212 and Trp-134), the quenching of which after treatment with NMOFs could be ascribed to the interaction between them (Fig. 2A and Fig. S1 in Supporting information) [32]. The adsorption of BSA on NMOFs surfaces may be driven by the proposed interaction, leading to protein corona formation. Thus, the zeta potential of NMOFs with BSA incubation was measured to investigate the BSA adsorption. As shown in Fig. 2B, as the addition of BSA with higher concentration, the surface potential of NMOFs markedly decreased, gradually closing to zeta potential of free BSA, indicating the increasing BSA adsorption amount on NMOFs surface.

To further demonstrate the protein corona of NMOFs, the XPS spectra were employed to analyze the interaction type and surface element composition. No change of the elements chemical shift before and after adsorption was exhibited, suggesting that the protein corona formation process was a non-chemical adsorption with no chemical bonds involved (Fig. 2C). Besides, the surface element composition of NMOFs were quantitively analyzed (Fig. S2 in Supporting information). According to the abovementioned results, the protein corona consisting of BSA could be formed on NMOFs surface. After protein corona formation, the contents of N element increased while that of Zr element decreased on the surface of NMOFs. Since N and Zr indicated the presence of BSA and NMOFs, the change of element content meant that the surface of NMOFs was coated by BSA. In addition, according to the variation difference of N and Zr content of NMOFs, it seemed that the surface BSA coating capacity followed the rank of UIO66 > UIO66-NH_2 > UIO66-2COOH. Then, with the removal of free BSA and soft protein corona, the hard protein corona coated NMOFs were recovered to analyze the protein corona formation. Preliminarily, the Raman spectra of NMOFs were collected to analyze the molecular structure of protein corona coated NMFs (Fig. S3 in Supporting information). No significant differences between NMOFs and NMOFs + BSA were found in UIO66 and UIO66-NH_2 groups, suggesting less protein corona formation on NMOFs. However, compared to bare UIO66-2COOH, the characteristic peak of BSA at 2929 cm^{-1} was clearly shown in protein corona coated samples, implying intense protein adsorption. To further accurately quantify BSA amount of the hard protein corona, the BCA assay was carried out. As shown in Fig. 2D, compared to UIO66 group, the relative BSA amount adsorbed on NMOFs surface was increased by 4.81 times in UIO66-2COOH group, while it was reduced by 18.79% in UIO66-NH_2 group.

According to the abovementioned results, the protein corona consisting of BSA could be formed on NMOFs surface. However, it is confusing that the surface BSA coating capacity follows the rank of UIO66 > UIO66-NH_2 > UIO66-2COOH while the BSA bind-

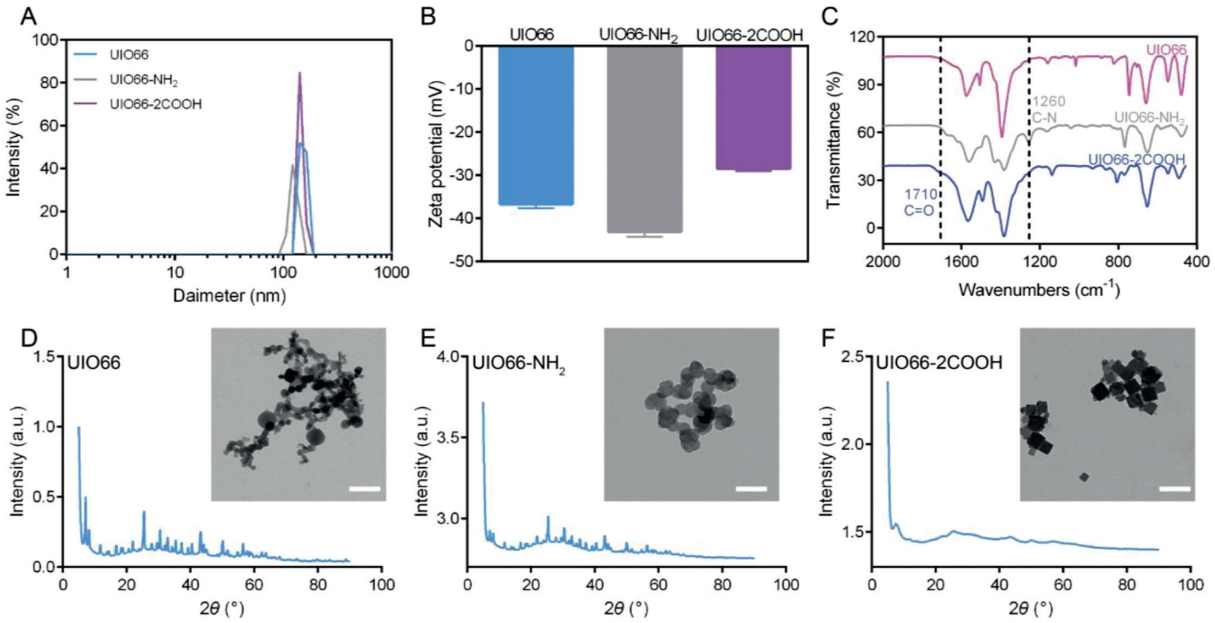

Fig. 1. Characterization of NMOFs: Size distribution (A) and surface zeta potential (B) of NMOFs. (C) The FTIR spectra of NMOFs. The PXRD spectra and TEM images of UIO66 (D), UIO66-NH_2 (E) and UIO66-2COOH (F). Scale bar = 200 nm. Data are expressed as mean ± SD, $n = 3$.

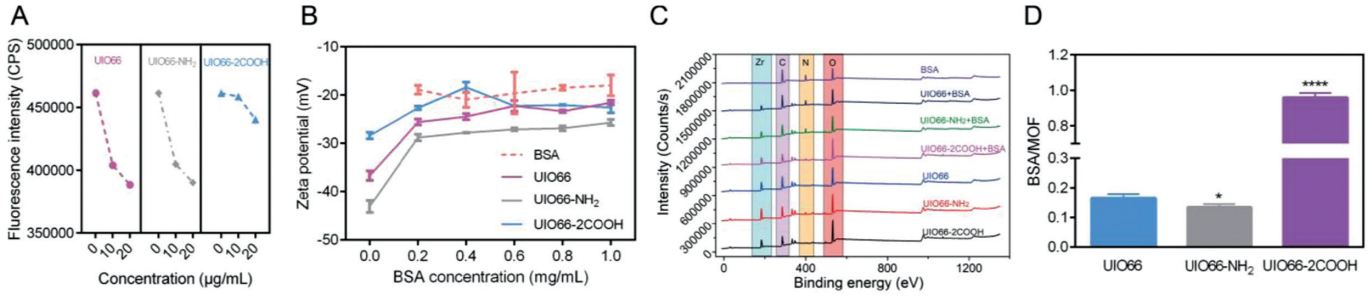

Fig. 2. BSA adsorption on NMOFs: Fluorescence intensity decrement of BSA as incubation with NMOFs (A); The zeta potential of NMOFs as addition of BSA of different concentrations (B); XPS spectra of NMOFs before and after incubation with BSA (C); Hard protein corona amount determined by BCA assay (D); Data are expressed as mean ± SD, $n = 3$.

ing amounts follow the different rank of UIO66-2COOH > UIO66 > UIO66-NH_2. To further figure out this difference, the interactions between BSA and NMOFs were analyzed accurately by microscale thermophoresis (MST) assay [33]. As shown in Figs. 3A-C and Fig. S4 (Supporting information), the dissociation constant (K_d) of BSA with UIO66 was determined to be 32.64 nmo/L, which corresponded to binding constant K_b of 3.06×10^7 L/mol. With the organic ligand modification of -NH_2, the K_d of BSA increased to be 54.316 nmol/L while K_b reduced to 1.84×10^7 L/mol, suggesting about 39.87% reduction of binding affinity between NMOFs and BSA, which might be ascribed to the weaker electrostatic interaction induced by the larger zeta potential. However, the binding affinity K_b remarkably increased from 3.06×10^7 L/mol to 2.27×10^{11} L/mol with organic ligand modification of -COOH, indicating the 7418 times increment of BSA adsorption ability. Thus, the highest BSA binding affinity of UIO66-2COOH can be concluded while the UIO66-NH_2 exhibits the weakest BSA adsorption ability, which is in line with the BSA adsorption amount measurements.

To rationalize the contradiction between NMOFs-BSA binding affinity and surface BSA coating capacity, we speculated that different protein corona formation modes dominated in modified NMOFs. Combined with the representative porous morphological characteristic of NMOFs, the surface coating mode (weak affinity) and porous embedded mode (strong affinity) were presented in our study. When surface coating mode play the major role, the BSA were mainly adsorbed on the frameworks rather than the pores, exhibiting weak binding affinity, significantly changing the surface elements compositions. However, when porous embedded mode dominates in the protein adsorption process, the BSA were mostly hidden inside the pores, exhibiting strong binding affinity, thus exerting less influence on surface elements composition of NMOFs. According to our hypothesis, it can be inferred that the porous embedded mode dominates in UIO66-2COOH group while surface coating mode rules in UIO66 and UIO66-NH_2 groups (Fig. 3D).

To confirm our speculation, the surface area of NMOFs was determined to clarify the porous difference after protein corona formation (Fig. 3E). Interestingly, with protein corona formation, the negligible surface area difference was found in UIO66 and UIO66-NH_2 groups, while the surface area of UIO66-2COOH was significantly reduced. The reduced surface area may represent that the distributed pores on UIO66-2COOH were largely occupied by proteins, indicating the embedded mode of BSA dominates in the UIO66-2COOH group. However, in the other two groups, the trivial change of surface area could be ascribed to the surface coating mode of BSA in protein corona formation process. This difference could also be evidenced by spectrum properties of BSA. As the adsorption peaks at 280 nm referring to the aromatic amino acids (Trp, Tyr, and Phe), UV–vis spectra of protein were widely employed to analyze the real-time status changes [32]. As illustrated in Fig. S5 (Supporting information) and Fig. 3F, as time went

by, the Abs of BSA at 280 nm was gradually increasing in UIO66 and UIO66-NH_2 groups while decreasing in UIO66-2COOH group. The hyperchromic shift for BSA might be correlated to the partial exposure of photon adsorbing amino acid residues, indicating the conformational change of BSA upon interaction with UIO66 and UIO66-NH_2 in a surface coating mode [14]. In contrast, the embedded BSA in the porous structure of UIO66-2COOH might result in the wrapping and hiding of these amino acid residues, which in turn led to the reduced Abs values. In addition, the porous structures of UIO66-2COOH may protect the BSA hidden in, endowing the less fluorescence quenching rate of proteins (Fig. 2A). In summary, the different protein corona formation modes were proved in NMOFs, where UIO66 and UIO66-NH_2 groups displayed surface coating mode and UIO66-2COOH obeyed porous embedded mode.

To fully understand the reason for these two protein corona formation modes, the N_2 adsorption isotherms were measured to elucidate the porous structures (Figs. 3G-I). It was shown that UIO66 and UIO66-NH_2 exhibited I-type adsorption isotherms, while UIO66-2COOH exhibited IV-type adsorption isotherms. The different adsorption of N_2 at low P/P^0 indicated the micropores structure (<2 nm) of UIO66 and UIO66-NH_2 and the mesoporous structure (2–50 nm) of UIO66-2COOH [20]. As the scale of a single BSA was about 6 nm [34], the mesoporous structures other than the microporous structures are more susceptible to being embedded by BSA. Thus, after protein corona formation, the adsorption isotherms of UIO66-2COOH decreased significantly, evidencing the protein embedment inducing porosity reduction. Quantitative results also confirmed that a 14.51% reduction of pore volume in UIO66-2COOH group, compared to 4.63% (UIO66) and 2.74% (UIO66-NH_2) in the other two groups, respectively. As indicated by the current results, the UIO66 and UIO66-NH_2 exhibit surface coating mode in protein corona formation process, where -NH_2 modification reduced the BSA adsorption capacity due to the weaker electrostatic interaction. However, the mesoporous structure of UIO66-2COOH leads to the unique porous embedded protein corona formation mode, causing the stronger BSA binding affinity, forming an intense hard protein corona, probably bringing a different impact.

It was widely reported that the protein corona formation on NPs may induce structural changes of NPs and conformational differences of proteins [35,36]. Thus, the crystal phase of NMOFs and secondary structures of BSA was investigated. The PXRD spectra of NMOFs were collected and shown in Figs. S6A-C (Supporting information). Compared to bare NMOFs, no visible change could be observed in protein corona coated NMOFs, indicating no considerable effect of protein adsorption on the crystal phase of NMOFs. However, the CD spectra showed that the secondary structure of BSA was slightly changed after interaction with NMOFs (Figs. S6D and E in Supporting information). The CD values at 208 nm, which reflected the content of α-helix in proteins, were gradually decreased with the increment of NMOFs concentrations in all groups, implying the improvement of α-helix content in BSA secondary structures. Compared to the other two groups, the degree of BSA conformational change in UIO66-2COOH group was much smaller, further verifying the protection effect of porous embedded mode (Fig. S7 in Supporting information). These results collectively elaborated the α-helix content increment of BSA in NMOFs protein corona, which might be ascribed to the unfolding of polypeptide chains.

In order to investigate the effect of protein corona formation on cellular uptake, the intracellular NMOFs species were detected by CLSM. As NMOFs were widely employed in biomedical materials for tumor therapy [18], the human non-small cell lung cancer cell A549 was chosen as a model cell line. Firstly, the cell toxicity of NMOFs was determined and the results were shown in Fig. S8 (Supporting information). It could be indicated that all the NMOFs group exhibit over 80% cell viability even at a high concentration of 1 mg/mL, demonstrating the great safety of these NMOFs. Then, the NMOFs were subjected to A549 cells culture medium containing different amounts of FBS, the multiple protein complexes including BSA. After removal of free NMOFs, the cell nuclei were stained with DAPI (blue) and the NMOFs were labeled with calcein (green) to observe the intracellular NMOFs. As shown in Fig. 4, with the increment of FBS content, the green signal of UIO66 and UIO66-NH_2 significantly decreased in A549 cells, indicating the protein corona induced cellular uptake reduction. The relative mean fluorescence intensity (MFI) of NMOFs decreased to about 33.46% and 17.51%, respectively. This phenomenon might be due to the surface hydrophilicity enhancement of NMOFs with BSA coating, which is consistent with other previous reports [10,37]. However, in UIO66-2COOH group, no significant A549 cell uptake difference was observed with 10% FBS addition, and the uptake reduction was only shown in 20% FBS group. Compared to the other two groups, about 54.09% MFI of NMOFs were recorded, suggesting the relatively minor impact of protein corona on cellular uptake of UIO66-2COOH. Presumably, the proteins in FBS may firstly occupy the pores following the porous embedded mode, which did not exert enough effect on UIO66-2COOH NMOFs surface chemistry to reduce the cellular uptake level. Nevertheless, with larger amounts of proteins were added, the surface coating mode may also participate in the protein corona process, influencing the surface hydrophilicity of NMOFs, thus attenuating the cellular internalization. Hence, it can be deduced that the surface coating of protein corona other than the porous embedded plays a critical role in cellular uptake reduction of NMOFs. The organic ligand modification of -COOH could be employed as a promising strategy to reduce the effect of protein corona formation on cellular uptake.

In this study, we explored the interaction between BSA and NMOFs to clarify the impact of organic ligand modifications on protein corona formations. The current results clearly demonstrate that the organic ligand modification remarkably affects the porous structures of NMOFs, where UIO66-2COOH exhibits mesoporous structure while UIO66 and UIO66-NH_2 exhibit micropores structure. The larger pore size allows UIO66-2COOH NMOFs to adsorb more BSA into its porous structure with the highest binding affinity, and the protein corona formation was mainly governed by porous embedded mode. Thus, as the protection function of micropores embedded, the spectrum properties and secondary structures of BSA could be maintained to a certain extent. The smaller impact of protein corona on cellular uptake level was also proved. However, with the modification of -NH_2, the BSA adsorption affinity and amount on NMOFs was slightly decreased, which is believed to be attributed to weaker electrostatic interaction between them. The protein corona formation on UIO66 and UIO66-NH_2 was dominated by surface coating mode, which significantly altered the BSA properties and structures. Thereto, it is considered that BSA coating increased the surface hydrophilicity of NMOFs, subsequently reducing the cellular uptake. Besides, the different protein corona formation modes did not affect the crystal phase of NMOFs, and no chemical bond was involved in the adsorption process. In summary, the protein corona formation process and its effects were prominently affected by organic ligand modifications.

NMOFs is a promising biomedical platform for drug delivery and therapeutic applications, which have been widely reported in many fields [18]. Although the great therapeutical effect of NMOFs was confirmed in recent publications [16,26], little attention has been paid to the detailed investigations of their specific fate when administrated *in vivo*. Herein, based on our research, the proteins in biological fluids may inevitably be adsorbed on the NMOFs, exerting a stunningly huge impact on their biological functions. Our further works would be performed to study the protein corona formations of NMOFs in complex biological fluids to simulate the real *in vivo* environment. The possible proteins competing-inducing

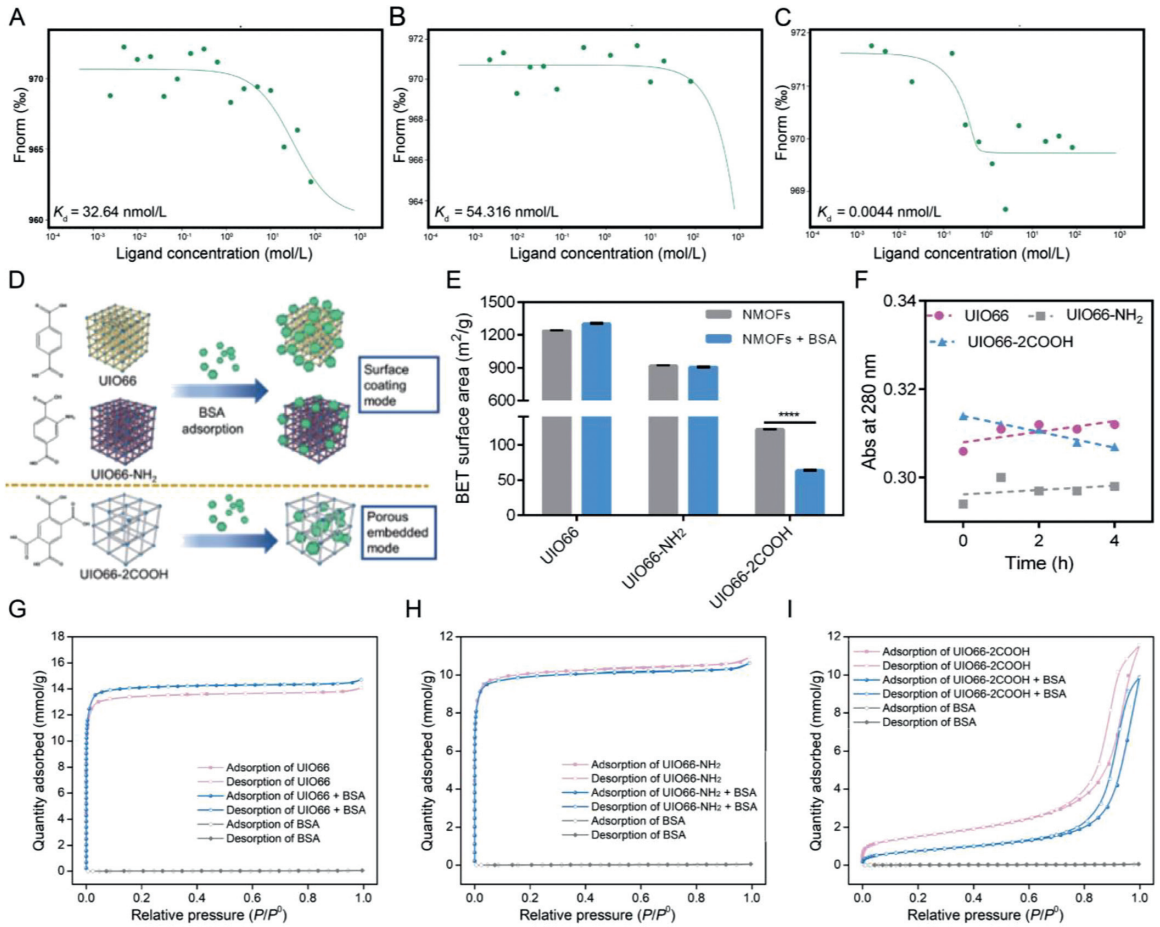

Fig. 3. Protein corona formation mode of NMOFs: Dose-response curves and fitted K_d values of UIO66 (A), UIO66-NH_2 (B) and UIO66-2COOH (C); The scheme of different protein corona formation modes of NMOFs with organic ligand modification (D); The BET surface area of NMOFs before and after protein corona formation (E); Absorbance at 280 nm of BSA incubated with NMOFs in different time intervals (F). The adsorption isotherms of UIO66 (G), UIO66-NH_2 (H) and UIO66-2COOH (I). Data are expressed as mean ± SD, $n = 3$, $^{****}P < 0.0001$.

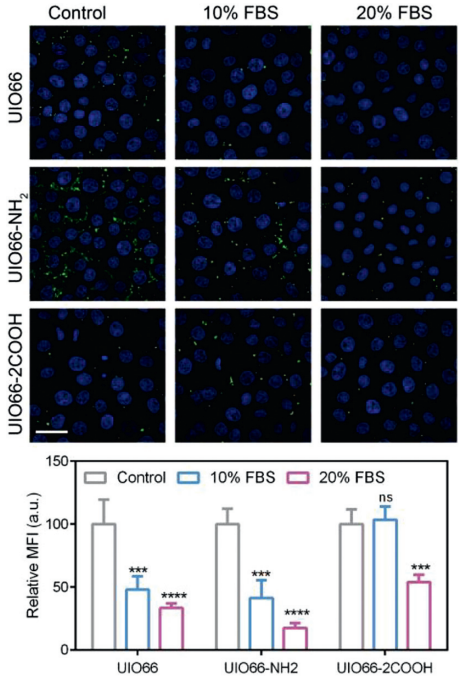

Fig. 4. Cellular uptake of NMOFs: The CLSM images of A549 uptake of NMOFs at different FBS concentrations and the corresponding relative MFI. Scale bar = 50 μm. Data are expressed as mean ± SD, $n = 3$, $^{***}P < 0.001$, $^{****}P < 0.0001$. ns, no significance.

drug leakage from porous structures should be taken into consideration, and the influence of protein corona on drug accumulation and metabolism should be emphasized. Our study provides a new insight to the design and employment of NMOFs in the drug delivery field.

Declaration of competing interest

The authors declare that they have no known competing financial interests or personal relationships that could have appeared to influence the work reported in this paper.

Acknowledgments

The authors would like to acknowledge the project grants from the National Natural Science Foundation of China (No. 82104070), the Key Areas Research and Development Program of Guangdong Province (No. 2019B020204002), and the Fundamental Research Funds for the Central Universities (No. 21621012).

Supplementary materials

Supplementary material associated with this article can be found, in the online version, at doi:10.1016/j.cclet.2022.02.052.

References

[1] W. Poon, B.R. Kingston, B. Ouyang, et al., Nat. Nanotechnol. 15 (2020) 819–829.
[2] S. Li, M. Li, S. Huo, et al., Adv. Mater. 33 (2021) 1–10.

[3] M. Chen, D. Yang, Y. Sun, et al., ACS Nano 15 (2021) 3387–3401.
[4] G. Erel-Akbaba, L.A. Carvalho, T. Tian, et al., ACS Nano 13 (2019) 4028–4040.
[5] B. Li, T. Chu, J. Wei, et al., Nano Lett. 21 (2021) 2588–2595.
[6] B. Wu, J. Fu, Y. Zhou, et al., Acta Pharm. Sin. B 10 (2020) 2198–2211.
[7] M. Cao, R. Cai, L. Zhao, et al., Nat. Nanotechnol. 16 (2021) 708–716.
[8] R. Cai, C. Chen, Adv. Mater. 31 (2019) 1–13.
[9] I. Lynch, A. Salvati, K.A. Dawson, Nat. Nanotechnol. 4 (2009) 546–547.
[10] Y. Yan, K.T. Gause, M.M.J. Kamphuis, et al., ACS Nano 7 (2013) 10960–10970.
[11] L. Wang, S.Y. Li, W. Jiang, et al., ACS Appl. Mater. Interfaces 12 (2020) 32312–32320.
[12] B.E. Givens, E. Wilson, J. Fiegel, Colloids Surf. B: Biointerfaces 179 (2019) 374–381.
[13] L. Guo, T. Wang, Z. Chen, et al., Chin. Chem. Lett. 29 (2018) 1291–1295.
[14] G. Wang, W. Wang, E. Shangguan, S. Gao, Y. Liu, Mater. Sci. Eng. C 111 (2020) 110830.
[15] W. Wang, Z. Huang, Y. Li, et al., Acta Pharm. Sin. B 11 (2021) 1030–1046.
[16] M.X. Wu, Y.W. Yang, Adv. Mater. 29 (2017) 1–20.
[17] Q.Y. Xu, Z. Tan, X.W. Liao, C. Wang, Chin. Chem. Lett. 33 (2021) 22–32.
[18] T. Wen, G. Quan, B. Niu, et al., Small 17 (2021) 2005064.
[19] E. Ploetz, A. Zimpel, V. Cauda, et al., Adv. Mater. 32 (2020) 1907267.
[20] N. Gan, Q. Sun, L. Zhao, et al., Int. J. Biol. Macromol. 140 (2019) 709–718.
[21] S. Jafari, Z. Izadi, L. Alaei, et al., Sci. Rep. 10 (2020) 1–14.
[22] S. Rojas, F.J. Carmona, C.R. Maldonado, et al., Inorg. Chem. 55 (2016) 2650–2663.
[23] J.S. Kahn, L. Freage, N. Enkin, M.A.A. Garcia, I. Willner, Adv. Mater. 29 (2017) 1–6.
[24] Z. Fan, H. Liu, Y. Xue, et al., Bioact. Mater. 6 (2021) 312–325.
[25] P. Gao, R. Lou, X. Liu, et al., Anal. Chem. 93 (2021) 5437–5441.
[26] J.H. Cavka, S. Jakobsen, U. Olsbye, et al., J. Am. Chem. Soc. 130 (2008) 13850–13851.
[27] L.L. Tan, H. Li, Y. Zhou, et al., Small 11 (2015) 3807–3813.
[28] P. Zhang, Y. Ouyang, Y.S. Sohn, et al., ACS Nano 15 (2021) 6645–6657.
[29] I. Abánades Lázaro, C.J.R. Wells, R.S. Forgan, Angew. Chem. Int. Ed. 59 (2020) 5211–5217.
[30] J.H. Cavka, S. Jakobsen, U. Olsbye, et al., J. Am. Chem. Soc. 130 (2008) 13850–13851.
[31] Y. Wang, Y. Qiu, A. Sun, et al., Anal. Chim. Acta 1133 (2020) 109–118.
[32] G. Wang, C. Yan, S. Gao, Y. Liu, Mater. Sci. Eng. C 103 (2019) 109856.
[33] O. Vilanova, J.J. Mittag, P.M. Kelly, et al., ACS Nano 10 (2016) 10842–10850.
[34] F. Fu, Z. Huang, W. Wang, et al., J. Drug Deliv. Sci. Technol. 64 (2021) 102376.
[35] S. Dominguez-Medina, L. Kisley, L.J. Tauzin, et al., ACS Nano 10 (2016) 2103–2112.
[36] R. del Caño, L. Mateus, G. Sánchez-Obrero, et al., J. Colloid Interface Sci. 505 (2017) 1165–1171.
[37] Q. Peng, S. Zhang, Q. Yang, et al., Biomaterials 34 (2013) 8521–8530.